



## Water Resources Research

### RESEARCH ARTICLE

10.1002/2015WR018016

#### Key Points:

- High spatial variability of land surface states in daily flux footprint
- Improved land-atmosphere coupling when footprint variability accounted for
- Footprint vegetation composition affects evapotranspiration and its partitioning

#### Correspondence to:

E. R. Vivoni,  
vivoni@asu.edu

#### Citation:

Anderson, C. A., and E. R. Vivoni (2016), Impact of land surface states within the flux footprint on daytime land-atmosphere coupling in two semiarid ecosystems of the Southwestern U.S., *Water Resour. Res.*, 52, doi:10.1002/2015WR018016.

Received 20 AUG 2015

Accepted 3 JUN 2016

Accepted article online 6 JUN 2016

## Impact of land surface states within the flux footprint on daytime land-atmosphere coupling in two semiarid ecosystems of the Southwestern U.S.

Cody A. Anderson<sup>1</sup> and Enrique R. Vivoni<sup>1,2</sup>

<sup>1</sup>School of Sustainable Engineering and the Built Environment, Arizona State University, Tempe, Arizona, USA, <sup>2</sup>School of Earth and Space Exploration, Arizona State University, Tempe, Arizona, USA

**Abstract** Land surface states play important roles in the turbulent exchanges between ecosystems and their overlying atmosphere. Field methods to estimate turbulent fluxes have time-variable source areas, while land surface observations are typically obtained at single plots with a smaller measurement scale. In this study, we characterize land-atmosphere interactions in two semiarid ecosystems in the southwestern U.S. At each study site, we combine the eddy covariance method with a distributed network of soil moisture and temperature sensors, high-resolution imagery of the spatial distribution of vegetation and soil patches, and novel spatiotemporal analyses to characterize the turbulent flux footprint analytically and identify the soil moisture, temperature, and vegetation conditions underlying the eddy covariance measurements. Four methods for aggregating the land surface observations to the scale of the daily flux footprint are tested. Our results reveal a large degree of spatial variability in the footprint, with stronger variations in soil moisture than in soil temperature. Single plot measurements are less reliable than the distributed network in capturing footprint conditions, particularly for soil moisture. Furthermore, a marked improvement is observed in the relations between turbulent fluxes and land surface states for methods capturing the footprint variability. We also identify that the composition of vegetation and soil patches in the time-variable source area affects the relative magnitudes of the turbulent fluxes and the partitioning of evapotranspiration. Our study points to the importance of monitoring the spatial distribution of land surface states (e.g., soil moisture and temperature) and vegetation and soil patches when assessing land-atmosphere interactions.

### 1. Introduction

Land-atmosphere interactions mediate the exchanges of momentum, heat, water, and gases between ecosystems and their overlying atmosphere. The conditions of the land surface in terms of its soil water content and temperature play important roles in these exchanges over a wide range of climate settings [e.g., Blanken *et al.*, 2001; Dettò *et al.*, 2006; Williams and Albertson, 2004; Alfieri *et al.*, 2007; Baldocchi, 2008]. Nevertheless, relations between turbulent fluxes and land surface states are typically assessed using measurements at disparate spatial scales. For example, various field methods to estimate evapotranspiration have time-variable source areas [e.g., Schmid, 2002; Evett *et al.*, 2012], while the soil moisture observations related to water vapor fluxes are made at single plots whose measurement scale is much smaller [e.g., Running *et al.*, 1999; Kurc and Small, 2007; Vivoni *et al.*, 2008a]. Furthermore, measurement methods used for turbulent fluxes, such as the eddy covariance (EC) technique, aggregate these fluxes within their source areas to obtain spatially averaged exchanges [Baldocchi *et al.*, 1988; Marcolla and Cescatti, 2005; Dettò *et al.*, 2006; Li *et al.*, 2008]. In theory, aggregated fluxes should be compared to the “effective” or spatially averaged conditions within the source area, but in practice the spatial variability of these conditions is often ignored.

With the wide adoption of the EC method, it is important to determine if single plots are representative of the conditions found within the source area (or turbulent flux footprint). Along these lines, Alfieri and Blanken [2012] compared EC measurements from a fixed and a mobile tower in a semiarid sagebrush ecosystem. During the course of a summer, the authors showed that heterogeneities in soil water content and leaf area index in the small sampling area ( $\sim 64 \times 64$  m) impacted the partitioning of available energy into sensible (H) and latent ( $\lambda ET$ ) heat fluxes. Similarly, large spatial variations in land surface states are expected

in other arid and semiarid ecosystems as these are characterized by vegetated and bare soil patches of varying size [e.g., *Scholes and Archer*, 1997; *Huxman et al.*, 2005]. For instance, *Detto et al.* [2006] quantified how the spatial distribution of woody vegetation and bare soil patches in a semiarid savanna of Sardinia, Italy, affected EC measurements. The authors identified that the fraction of bare soil in the 50% source area had important implications on  $\lambda$ ET, in particular for a 2 month dry period. *Alfieri and Blaken* [2012] and *Detto et al.* [2006] show that common assumptions on spatial variability need to be carefully inspected when linking EC measurements to land surface states. While spatial variability has been inferred from coarse remote sensing data [e.g., *Gockede et al.*, 2004; *Gelybo et al.*, 2013], few studies to date have utilized ground-based observations to characterize the land surface conditions in the turbulent flux footprint.

The patchiness of arid and semiarid ecosystems is further complicated by the dynamic nature of plant communities. For example, woody plant encroachment is a phenomenon in the southwestern U.S. and elsewhere [e.g., *Burrows et al.*, 1990; *Van Auken*, 2000; *Archer et al.*, 2001; *Silva et al.*, 2001; *Huenneke et al.*, 2002; *Huxman et al.*, 2005; *Browning et al.*, 2008] in which a conversion occurs from desert grasslands to alternate ecosystem states, such as savannas or shrublands, dominated by trees or shrubs. In these systems, spatial patterns of grasses, woody plants, and bare soil patches evolve over time (seasons to decades) from the interactions between climate, terrain, and soil effects on water availability, as well as resource competition, herbivory, and fire [*D'Odorico et al.*, 2012]. In addition, seasonal to interannual variations in the phenology of individual species in a plant community can have important consequences on resource availability [*Reynolds et al.*, 1999; *Chesson et al.*, 2004; *Ogle and Reynolds*, 2004]. Furthermore, the proportion of bare soil will vary in time as a function of the life and phenological stages of competing plants, in particular for herbaceous species with a rapid response to water availability.

For ecosystems in the Sonoran and Chihuahuan Deserts, vegetation phenology is strongly linked to precipitation during the summer months (July–September) associated with the North American monsoon. In response to available water, plant communities generally increase their net primary productivity and as a consequence their contribution to the evapotranspiration (ET) from the ecosystem. Various methods have been applied to quantify the contributions of plant transpiration (T) and soil evaporation (E) to the total ecosystem ET, including stable isotope techniques [*Williams et al.*, 2004; *Yépez et al.*, 2007], empirical methods using soil, plant, and meteorological data [*Scott et al.*, 2006; *Moran et al.*, 2009], and modeling approaches [*Vivoni*, 2012; *Méndez-Barroso et al.*, 2014]. Nevertheless, challenges exist in characterizing the bare soil and vegetation contributions to evapotranspiration in arid and semiarid ecosystems. Given the spatial variability in the time-variable source area [e.g., *Detto et al.*, 2006; *Vivoni et al.*, 2010; *Alfieri and Blaken*, 2012], it is important to quantify how ET partitioning is linked to land surface conditions at a similar spatial averaging scale as the direct EC measurements.

In this study, we characterize the relation between turbulent fluxes and the land surface states within the time-variable source area in two semiarid ecosystems that are representative of the Sonoran and Chihuahuan Deserts. Both ecosystems have undergone the process of woody plant encroachment and consist of assemblages of tree or shrub patches, herbaceous cover and bare soil. At each study site, we combine turbulent flux measurements from the EC technique with (1) a distributed sampling network of soil moisture and temperature sensor profiles in the EC source area, (2) high-resolution imagery characterizing the distribution of vegetation and soil patches, (3) an empirical ET partitioning method of *Moran et al.* [2009], and (4) spatiotemporal analyses to characterize the turbulent flux footprint and its land surface states. We aim to answer the following: How do soil moisture and soil temperature conditions vary within the source area of EC measurements? Can evapotranspiration components within the flux footprint be related to the land surface conditions? and Does accounting for spatiotemporal variations of land surface states impact their relations with turbulent fluxes? Since this cross-site comparison integrates a number of data sets, we focus attention on quantifying land-atmosphere interactions from May to September 2013, spanning a monsoon season, by aggregating the flux footprint and land surface states for daytime conditions. While limited to two semiarid areas, this effort has implications for a wide range of ecosystems where turbulent fluxes need to be linked to land surface states.

## 2. Methods

### 2.1. Study Sites and Climate Characteristics

The two study sites are located in the Santa Rita Experimental Range (SRER), 45 km south of Tucson, Arizona, in the Sonoran Desert, and the Jornada Experimental Range (JER), 30 km north of Las Cruces, New

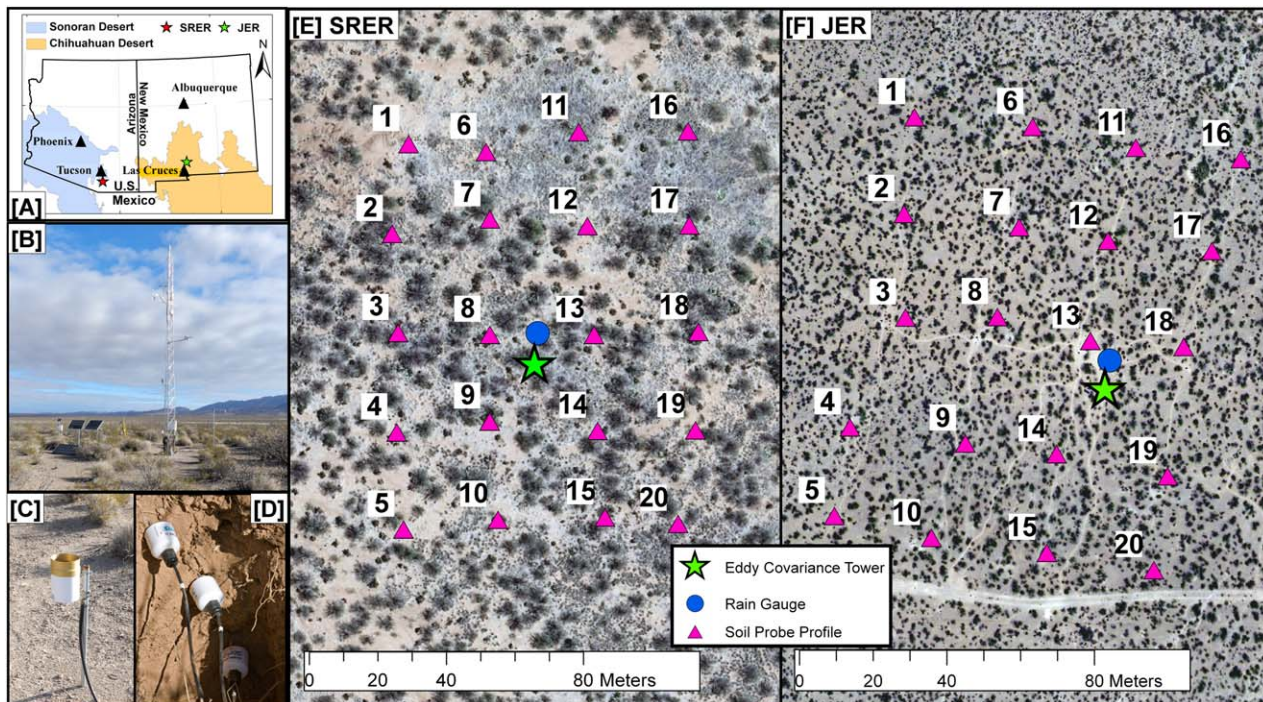


**Figure 1.** (A) Geographic location of the two study sites (SRER and JER) within the states (Arizona and New Mexico) and deserts (Sonoran and Chihuahuan) of the southwestern U.S. Photographs of the three main instruments: (B) eddy covariance tower, (C) tipping bucket rain gauge, and (D) soil moisture and temperature probe profiles. Instrumentation network at (E) SRER and (F) JER overlaid on aerial imagery from LiDAR and UAV approaches. SRER tower is at 3,520,198 m Northing and 514,121 m Easting in UTM Zone 12, while JER tower is at 3,606,405 m Northing and 349,526 m Easting in UTM Zone 13.

Mexico, in the Chihuahuan Desert (Figure 1A). Both rangeland sites have undergone a shift from semiarid grasslands to savannas or shrublands as part of the regional phenomenon of woody plant encroachment in the southwestern U.S. [Van Auken, 2000]. The sites were selected based on the availability of long-term data from the U.S. Department of Agriculture-Agricultural Research Service (USDA-ARS) used to study the woody plant encroachment process since 1903 (SRER) and 1911 (JER). More recently, Templeton *et al.* [2014] and Pierini *et al.* [2014] established eddy covariance towers in representative ecosystems of each rangeland (Figure 1B), along with a watershed instrumentation network.

Climate characteristics at the two study sites vary in accordance with their respective locations. Table 1 presents the monthly precipitation ( $P$ ) and air temperature ( $T_a$ ) obtained from long-term data sets at each site from May to September. SRER has hotter conditions due to its lower elevation (1170 m as compared to 1470 m at JER), while both sites exhibit most precipitation during the North American monsoon. Mean annual precipitation varies from 369 to 280 mm/yr at SRER and JER, with 55 and 51% occurring during the monsoon, in agreement with prior studies [Douglas *et al.*, 1993; Vivoni *et al.*, 2008a]. Climate conditions during May and June, prior to the monsoon, are hot and dry. In the study period, SRER received precipitation similar to the long-term average, while summer 2013 was wetter than average at JER, in particular for September. It is important to keep these comparisons in mind when inspecting the soil hydrologic conditions and land surface fluxes at the two sites during the study period.

## 2.2. Vegetation and Soil Characteristics

Vegetation at the study sites was characterized through high-resolution aerial imagery (Figures 1E and 1F) available from a light detection and ranging flight at SRER and an unmanned aerial vehicle flight at JER. Each orthoimage was aggregated to a matching 50 cm resolution and used to derive a vegetation map guided by identification of plant species [Anderson, 2013]. As shown in Figure 2, the resulting vegetation maps contain four and five dominant classes (shown with areal percentages) at SRER (grass [43.1%], velvet mesquite [28.2%], bare soil [23.3%], and prickly pear [5.5%]) and at JER (bare soil [64.3%], other shrubs [14.7%], creosote bush [7.6%], honey mesquite [7.3%], and grass [6.1%]), obtained for a 600 × 600 m area centered at each EC tower. Differences in bare soil are noteworthy, with JER having 3 times more bare soil

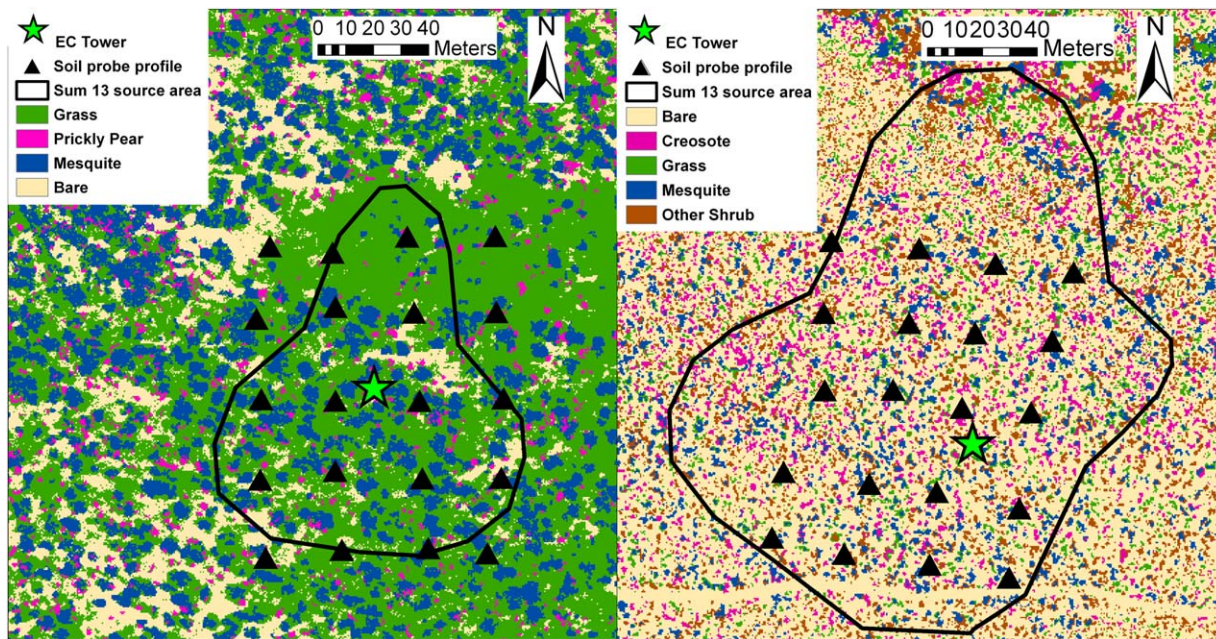


**Figure 2.** Vegetation classification maps at 50 cm resolution derived from orthoimages (Figures 1E and 1F), along with locations of soil moisture and temperature probe profiles and the 50% source areas of the EC towers for summer 2013 at SRER (left) and JER (right). At SRER, grass includes bush muhly (*Muhlenbergia porteri*), Lehmann lovegrass (*Eragrostis lehmanniana*), Santa Rita threeawn (*Aristida glaberrima*), and Rothrock grama (*Bouteloua rothrockii*), while mesquite refers to velvet mesquite trees (*Prosopis velutina* Woot.) and prickly pear (*Opuntia engelmannii*) is a cactus. At JER, grass includes bush muhly, tobosa grass (*Pleuraphis mutica*), and dropseed (*Sporobolus sp.*) and other shrubs includes mariola (*Parthenium incanum*), tarbush (*Florencea cernua*), and snakeweed (*Gutierrezia sarothrae*), while mesquite refers to honey mesquite shrubs. Bare soil is denoted as “Bare.”

cover, while SRER is primarily composed of velvet mesquite trees and grass species. As a result, vegetation patches tend to be larger and more organized at SRER, while JER is composed of smaller shrub patches that are more randomly distributed around the EC tower. This contrast in the spatial arrangement of plant and bare soil patches persists during the study period as vegetation green-up has little impact on cover amounts due to the lack of annual grasses and forbs.

The soils at the study sites were characterized at the distributed sampling plots shown in Figures 1E and 1F for depth ranges of 0–7, 7–17, and 17–27 cm using a split-tube corer. Particle size analysis was conducted to provide estimates of the gravimetric contents of gravel (three sizes), sand (five sizes), silt, clay, and the

**Table 1.** Measured Monthly Precipitation (P) and Evapotranspiration (ET), Along With Estimated Monthly Plant Transpiration (T), Soil Evaporation (E), and Transpiration Ratio (T/ET) for SRER and JER During the 2013 Study Period<sup>a</sup>

Site	Variable	Time Period					
		May	Jun.	Jul.	Aug.	Sep.	TOT
SRER	Long-term P (mm)	4.5	10.7	87.1	78.8	38.6	219.7
	P (mm)	0.0	9.7	92.7	85.6	32.8	220.8
	ET (mm)	7.6	9.5	39.1	55.5	21.6	133.3
	T (mm)	7.0	7.2	27.9	27.0	14.0	83.1
	E (mm)	0.5	2.3	11.2	28.5	7.6	50.1
	T/ET (%)	93	76	71	49	65	70.8
JER	Long-term T <sub>a</sub> (°C)	24.3	29.0	30.1	29.3	27.4	28.0
	Long-term P (mm)	13.8	21.2	51.1	57.8	33.2	177.1
	P (mm)	0.0	9.1	86.9	94.0	174.2	364.2
	ET (mm)	2.6	7.0	13.8	34.1	29.2	86.7
	T (mm)	0.8	1.7	9.1	22.7	20.7	55.0
	E (mm)	1.8	5.4	4.7	11.4	8.5	31.8
	T/ET (%)	30	24	66	67	71	51.6
	Long-term T <sub>a</sub> (°C)	23.2	27.5	28.2	26.7	23.8	25.9

<sup>a</sup>Long-term monthly average P and air temperature (T<sub>a</sub>) are shown for comparison. TOT represents the total (P, ET, T, and E) or average (T/ET and T<sub>a</sub>) amounts over May–September. SRER data were obtained from the USDA-ARS Southwest Watershed Research Center (1936–2011 for precipitation and 2004–2012 for air temperature), while JER data sets are both from the USDA-ARS Jornada Experimental Range (1983–2009).

**Table 2.** Comparison of Vegetation Cover Percentage in the Daily Flux Footprint for Varying Source Areas Over Averaged Conditions and for the Surrounding Landscape<sup>a</sup>

Site	Vegetation Cover (%)	Daily Flux Footprint for Different Source Areas			Landscape
		30%	50%	80%	
SRER	Bare	5.4	10.7 [5, 13]	17.6	23.3
	Grass	61.7	62.7 [55, 73]	53.9	43.1
	Mesquite	28.5	23.0 [14, 31]	23.5	28.2
	Prickly pear	4.3	3.6 [3, 6]	5.1	5.4
	JER	66.0	64.8 [60, 69]	64.2	64.3
JER	Grass	7.4	7.7 [4, 9]	8.7	6.1
	Mesquite	10.0	9.1 [8, 11]	7.1	7.3
	Creosote	8.2	8.5 [5, 10]	7.6	7.6
	Other shrubs	8.4	9.9 [9, 15]	12.4	14.7

<sup>a</sup>Brackets indicate minimum and maximum values for the 50% source area in the 2013 study period.

bulk density (entire sample and without gravels). Anderson [2013] reports on the detailed findings of the soil texture analysis. At SRER, the site is composed of loamy sand and sandy loam, while the soils at JER have a higher percentage of gravels and a texture that varies from sandy loam to silt loam due to a higher clay fraction.

### 2.3. Eddy Covariance Measurements and Distributed Sampling Network

An eddy covariance tower was installed at each site prior to this study to measure precipitation, meteorological variables, radiation components, and surface energy fluxes, as described in Pierini et al. [2014] and Templeton et al. [2014]. Measured turbulent fluxes were obtained using an open-path Infrared Gas Analyzer (LI7500, LI-COR) and three-dimensional wind velocity at 7 m (CSAT3, Campbell Sci.) aligned to the dominant wind direction toward the southwest at each site, sampled at a 20 Hz frequency and processed at 30 min intervals using EdIRE [Clement, 1999]. Other measurements were recorded as 30 min averages, including surface temperature at 1.5 m height (SI-111 Infrared Radiometer, Apogee), which has a small footprint area of  $\sim 0.3 \text{ m}^2$  with primarily a bare soil cover, with some overlapping plant species. Using EdIRE, standard corrections were performed following Scott et al. [2004], including the removal of signal lags and outliers (greater than  $\pm 4$  standard deviations from the mean) of gas concentrations [Massman, 2001]; rotating the coordinate frame to set the mean vertical wind speed to zero during each 30 min interval [Wilczak et al., 2001]; and corrections for density fluctuations [Webb et al., 1980]. We then applied a set of additional filters for periods with precipitation ( $>1 \text{ mm}/30 \text{ min}$ ) and when friction velocity  $<0.15 \text{ m/s}$ . Linear interpolation was used to fill gaps ( $<2 \text{ h}$ ) resulting from the quality-control procedures.

EC measurements were utilized to estimate the flux footprint using the analytical model of Kormann and Meixner [2001] for an area of  $600 \times 600 \text{ m}$  at 3 m resolution centered at each tower. The flux footprint was estimated at 30 min intervals during turbulent daytime conditions by setting a minimum  $H > 2 \text{ W/m}^2$ , a friction velocity  $>0.03 \text{ m/s}$ , and a stability parameter within  $\pm 30$  and averaged from sunrise to sunset. Design of the distributed sampling network was based on summer season footprint estimates prior to the deployment [Anderson, 2013] using the 50% source area (Figure 2). The 50% cutoff was selected due to constraints in the extent of the vegetation classification and practical limitations related to the installation of a distributed sampling network. A fetch analysis, defined as the maximum distance between the EC tower and source area extent, demonstrated that the 50% contour line is contained within the vegetation map 100 and 95% of the time at SRER and JER. A sensitivity analysis for much larger source areas revealed that the flux footprint exceeded the vegetation map during an unacceptable number of times. Nevertheless, comparison of the vegetation composition in the seasonally averaged footprints (30–80%) showed lower sensitivity at both sites among the footprints as compared to the surrounding landscape (Table 2). In addition, the uncertainty present in the daily cover estimates due to the selection of the source area threshold was low (0.5–4% at SRER and 0.9 and 1.3% at JER for the comparison between the 50 and 80% source areas). In the rare instances when the 50% contour extended beyond the vegetation map at JER, we assumed that the missing areas had a vegetation composition equal those in the entire image. In principle, the approach conducted here could be carried out with larger source areas (e.g., 80 and 90%), if land cover data is sufficiently extensive and the distributed network is designed to match the larger source area extent, two limitations of the present study.

Based on the summer season footprints, we installed a distributed sampling network to capture the spatial variability of soil moisture and temperature conditions around the EC tower. The 50% source areas provided the spatial extents (~120 m in N-S direction and ~90 m in E-W direction) from which we selected a  $5 \times 4$  grid pattern at 30 m spacing as the most efficient sampling approach given logistical and cost constraints. Four north-south transects consisting of five profiles were utilized (Figures 1E and 1F) with each consisting of three soil dielectric sensors (Hydra Probe, Stevens Water) at 5, 15, and 30 cm depths (Figure 1D). Sensors measure the impedance of an electric signal through a 40.3 cm<sup>3</sup> soil volume [Campbell, 1990] to determine the volumetric soil moisture ( $\theta$  in m<sup>3</sup>/m<sup>3</sup>) and soil temperature ( $T_s$  in °C) as 30 min averages. Sensor accuracy was stated by the manufacturer as 0.03 m<sup>3</sup>/m<sup>3</sup> and 0.6°C for soil moisture and soil temperature. A “loam” calibration equation was used in the conversion [Seyfried *et al.*, 2005] and corrected using relations established through gravimetric soil sampling at each study site [Anderson, 2013]. To match the flux footprint estimates, we averaged 30 min data over the daylight hours (6:00 A.M.–7:30 P.M.) for summer 2013. Depth averaging was performed over the intervals of 0–10, 0–20, and 0–40 cm using appropriate weighting of each sensor.

#### 2.4. Spatiotemporal Analysis Techniques and Land-Atmosphere Relationships

Measurements from the distributed sampling network formed the basis for characterizing soil moisture and temperature at each site. Basic statistical analyses were performed to obtain the daily spatial average and standard deviations across the 20 profiles at each depth (5, 15, and 30 cm) and for depth averages (0–10, 0–20, and 0–40 cm). Temporal averages and standard deviations were also obtained using daytime measurements. Data gaps related to sensor malfunction (~5% of sensors in any day) were not included in the averaging [Anderson, 2013]. Based on this information, four methods were utilized to represent the land surface conditions. To depict standard practices in land-atmosphere studies [e.g., Baldocchi *et al.*, 1988; Running *et al.*, 1999], we selected the nearest profile to the EC tower (labeled “Near”). Daily spatial (arithmetic) averages of the twenty profiles (“Mean”) provided a simple alternative to represent the conditions around the EC tower. Spatial interpolation of the twenty profiles using kriging [e.g., Delhomme, 1978] was performed to sample soil moisture and temperature in the daily flux footprint (“Footprint”). In this approach, the spatially interpolated field is weighted according to the 3 m pixel contributions in the 50% source area, with analyses for other source areas exhibiting small differences (i.e., 0.04–0.13°C in  $T_s$  and 0.001–0.003 m<sup>3</sup>/m<sup>3</sup> in  $\theta$ ). Finally, the sensor profile that best captures conditions in the flux footprint (“Monitor”) was found by applying time-stability analysis [e.g., Grayson and Western, 1998; Vivoni *et al.*, 2008b].

To complement the above, the areal cover of each vegetation class was found within the daily flux footprint and used to assess controls on the turbulent fluxes. Daytime totals of sensible heat flux ( $H$  in W/m<sup>2</sup>), latent heat flux ( $\lambda ET$  in W/m<sup>2</sup>), or evapotranspiration (ET in mm/d) and evaporative fraction (EF =  $\lambda ET / (\lambda ET + H)$ ) were related to the land surface conditions ( $\theta$  and  $T_s$ ) represented by each of the four methods using linear regressions. We used the quality-controlled  $H$  and ET measurements as directly obtained from the EC method and did not apply an energy balance correction, such as residual-LE closure [Twine *et al.*, 2000], which is justified by the open, heterogeneous vegetation cover where errors in the available energy can be significant [Lloyd *et al.*, 1997]. Relations between turbulent fluxes and land surface conditions were analyzed for two subsets during summer 2013—premonsoon and monsoon—determined based upon the arrival of storm events. To interpret relations between turbulent fluxes and land surface states, we applied regressions (i.e.,  $ET = f(\theta)$  as piecewise linear,  $H = f(T_s)$  as linear functions) based upon commonly assumed functions in hydrologic models [e.g., Laio *et al.*, 2001; Ivanov *et al.*, 2004] and ignored other contributing factors (e.g., vapor pressure deficit and air temperature). Due to the lack of direct measures of ET partitioning at the two sites, we adopted the approach of Moran *et al.* [2009] to provide a daily estimate of E/ET and T/ET using depth-averaged soil moisture and surface temperature ( $T_{sur}$ ) data. An improvement to the approach was applied by using soil moisture in the daily flux footprint rather than a single plot. Since the method ignores evaporation of intercepted water, rainy days (>5 mm) and its following day were excluded. A Student’s *t* test [Montgomery *et al.*, 2006] and a linear regression were used to test controls on the turbulent fluxes or ET partitioning for different vegetation compositions in the footprints.

### 3. Results and Discussion

#### 3.1. Spatiotemporal Variability of Land Surface Conditions

Land surface conditions in the daily flux footprint are expected to vary in time and space due to the interactions of rainfall events with soil and vegetation characteristics. As an example, Figure 3 shows the temporal

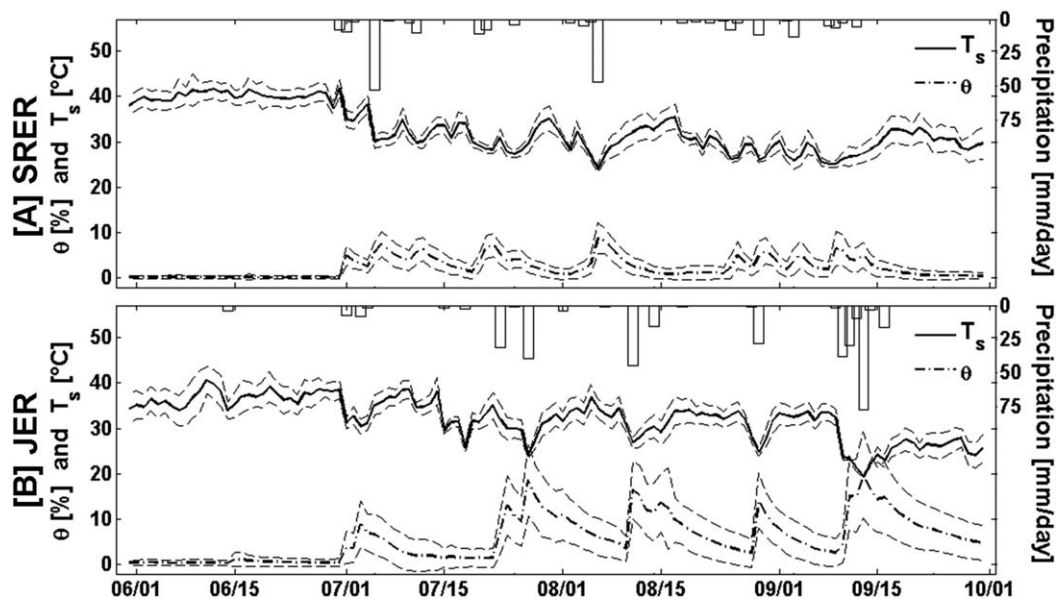


**Figure 3.** Precipitation (mm/d) and spatially averaged (“Mean”) soil moisture ( $\theta$  in %) and soil temperature ( $T_s$  in  $^{\circ}$ C) at 5 cm depth obtained as daytime averages at (A) SRER and (B) JER. The dashed line envelopes indicate the  $\pm 1$  spatial standard deviation.

variation of the spatially averaged soil moisture ( $\theta$ ) and temperature ( $T_s$ ) at 5 cm depth at SRER and JER, obtained as daytime averages. The arithmetic spatial average (“Mean” of 20 plots) is shown, along with the  $\pm 1$  spatial standard deviation. Note that the onset and duration of the North American monsoon are approximately the same at the two sites, resulting in large increases in  $\theta$  and decreases in  $T_s$  during the monsoon period. In response, a large shift is observed in the Bowen ratio ( $B = H/\lambda ET$ ) from high values prior to the monsoon onset (mid-day  $B$  from 10 to 70) to lower ranges during the monsoon ( $B = 0.2\text{--}8$  at SRER and  $B = 0.1\text{--}30$  at JER). Averaged over time, wetter surface soils are present at JER (7.37%) as compared to SRER (3.10%) in response to the above-average rainfall at JER (Table 1), though soil temperatures are similar (30.99 $^{\circ}$ C at SRER and 31.35 $^{\circ}$ C at JER). Days between rainfall events exhibit a progressive decrease in  $\theta$  and an increase in  $T_s$ , as well as changes in the spatial variability ( $\pm 1$  standard deviation) in the distributed network. As a result, these days exhibit reductions in  $\lambda ET$  and increases in  $H$  (i.e., progressively higher  $B$ ) in response to the land surface conditions, following the behavior reported by Templeton *et al.* [2014] and Pierini *et al.* [2014].

To explore the spatial variability, Figure 4 shows representations of the temporal coefficient of variation (CV, or ratio of temporal standard deviation to mean) of  $\theta$  and  $T_s$  measured during daytime hours. Here, each symbol represents a particular sampling plot and depth (from left to right as 5, 15, and 30 cm) and depicts CV with different sizes. The maps show that variations in the CV of  $\theta$  and  $T_s$  occur in short distances around the EC towers in response to factors such as soil conditions and proximity to plant canopies. Overall, higher relative temporal variability is observed for soil moisture (CV from 0 to 4.0) than soil temperature (CV from 0 to 1.0) at both sites. In most cases, the CV of  $\theta$  and  $T_s$  are muted for the progressively deeper sensors that are more isolated from rainfall and solar radiation forcing. Interestingly, the spatial standard deviation (Figure 3) is higher at JER (7.66% for  $\theta$  and 7.21 $^{\circ}$ C for  $T_s$ ) than at SRER (3.60% for  $\theta$  and 5.27 $^{\circ}$ C for  $T_s$ ), indicating the presence of more varied land surface conditions at JER. This corresponds to a larger variation in space of the temporal CV at JER (Figure 4), likely due to the smaller size of bare soil and shrub patches and their more random distribution.

The large spatial variability around the EC towers suggests that single  $\theta$  and  $T_s$  sites might be inappropriate to characterize land surface conditions. To address this, we first utilize time-stability analysis to determine which sampling plots represent best the spatially averaged conditions. As an example, Figure 5 presents the mean relative difference (%) of depth-averaged (0–10 cm)  $\theta$  and  $T_s$  at SRER and JER. Mean values at the 20 sampling plots are ranked and shown with error bars depicting  $\pm 1$  standard deviation of the relative difference [Grayson and Western, 1998]. We modified the standard approach so that differences were calculated relative to the spatial average weighted by the footprint. Sampling plots with a mean relative

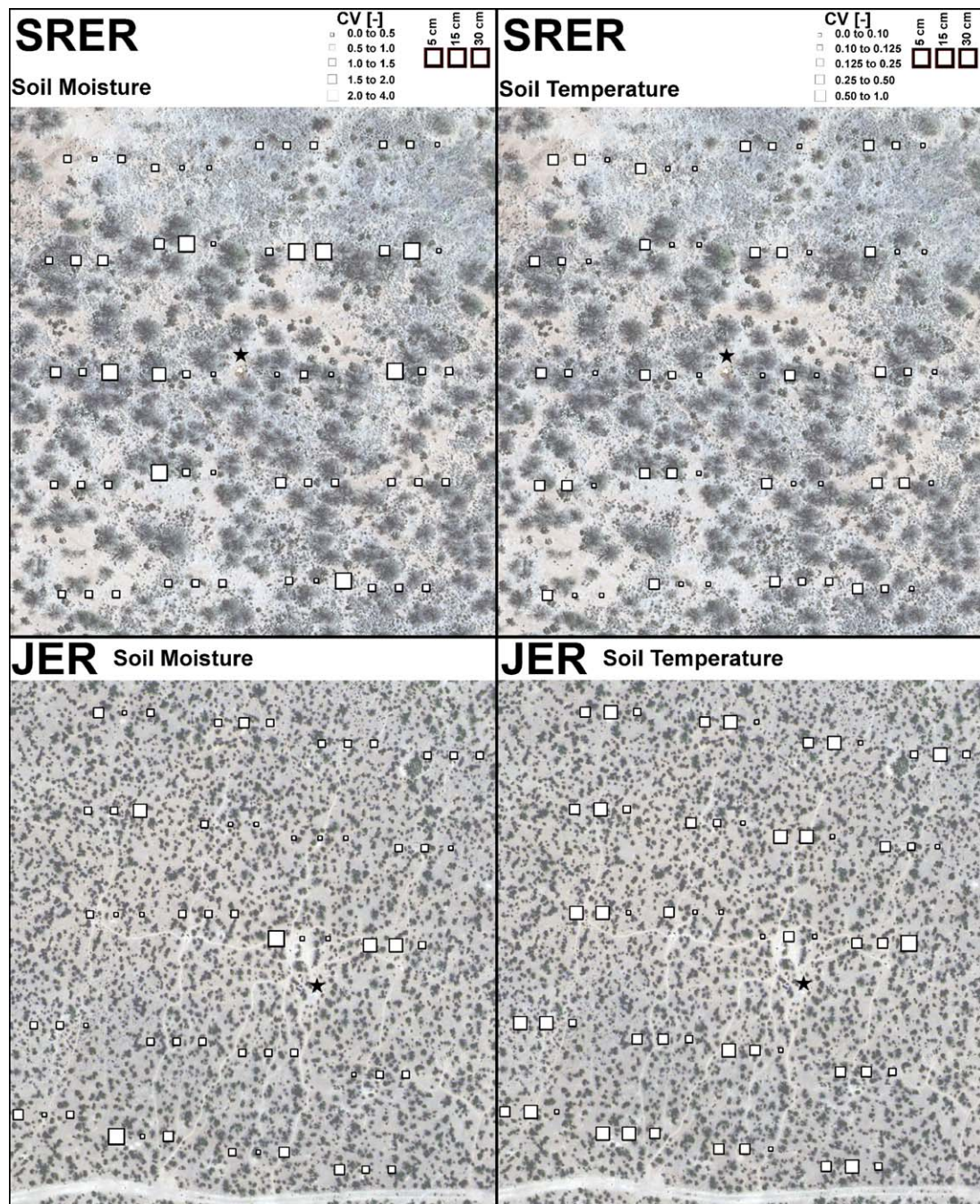


**Figure 4.** Temporal coefficient of variation (CV, dimensionless) of soil moisture ( $\theta$ ) and soil temperature ( $T_s$ ) at three depths at SRER (top) and JER (bottom) over the 2013 study period (1 May to 30 September). The magnitudes of CV (ratio of temporal standard deviation to temporal mean) are indicated by the size of the white squares, with the same legend used for both sites in each variable. Each set of three squares represents sensors located at 5, 15, and 30 cm depths, arranged from left to right and collocated at the center square. An offset is used here for clarity.

difference close to zero and a small standard deviation were selected as plots that monitor well the footprint ("Monitor"). Figure 5 shows how the relative differences of  $\theta$  with respect to the footprint average ( $-100$  to  $+300\%$ ) are much larger than for  $T_s$  ( $-6$  to  $+5\%$ ) at both sites, indicating that  $\theta$  exhibits a larger variability than  $T_s$ . Since relative differences are dampened with depth, it is likely that soil and vegetation factors affect the spatial variability of surface conditions to a greater extent than in deeper soils. The lower spatiotemporal variability in  $T_s$  also leads to a more consistent selection of "Monitor" plots as compared to  $\theta$  where the selection varied with depth.

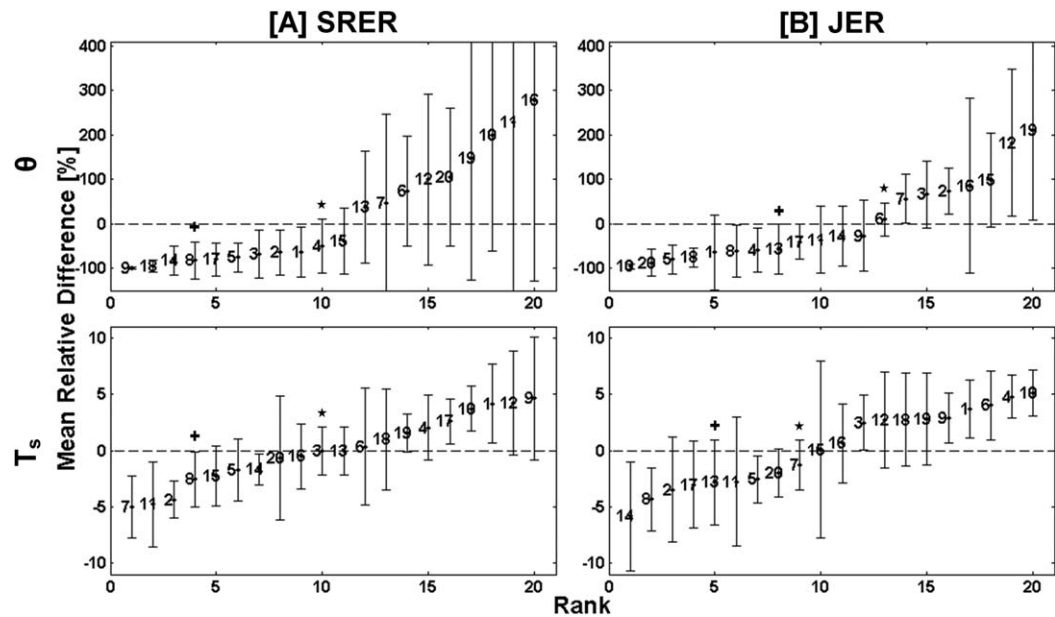


**Figure 5.** Ranked mean relative difference (%) of soil moisture ( $\theta$ , top) and soil temperature ( $T_s$ , bottom) for the 0–10 cm depth average at (A) SRER and (B) JER over the 2013 study period. Error bars represent the  $\pm 1$  standard deviation of the relative difference for each plot (each labeled with a plot number shown in Figure 1). Stars depict the selected “Monitor” plot for each panel and crosses indicate the “Near” plot in close proximity to the EC tower (#8 at SRER and #13 at JER).

Based on the time-stability analysis, Figure 6 compares measurements of depth-averaged  $\theta$  and  $T_s$  at the “Near” and “Monitor” plots to the spatially interpolated average conditions in the daily flux footprint (“Footprint”). Each symbol in the scatterplots depicts a daytime average in the study period. Clearly, the “Monitor” plots are superior to measurements taken near the EC towers (plots 8 and 13 at SRER and JER) in representing land surface states in the time-varying footprint. Furthermore, the larger spatial variability in  $\theta$  as compared to  $T_s$  results in “Near” measurements that are substantially less reliable in capturing the footprint average. This implies that the selection of single representative plots near EC towers is more critical for soil moisture in these two ecosystems, consistent with analyses from Loescher *et al.* [2014] for a large number of ecosystems. For the relatively open savanna at SRER and mixed shrubland at JER, soil and vegetation differences in the distributed network lead to spatial variations in soil moisture that attenuate with soil depth. Limited shading results in less spatial variations in soil temperature such that locations near the EC towers provide an adequate depiction of the footprint average.

### 3.2. Footprint Characterization and Evapotranspiration Partitioning

The daily flux footprint varies in time according to the wind direction and speed [e.g., Hsieh *et al.*, 2000; Kormann and Meixner, 2001] and thus captures different soil and vegetation conditions in a heterogeneous landscape. This interaction can be quantified using the high-resolution vegetation maps since the spatial variation of vegetation was substantially higher than soil differences in the distributed network [Anderson, 2013]. Figure 7 depicts the vegetation cover percentage in each daily flux footprint during the study period and a comparison of two dates (18 and 30 July at SRER) for illustrative purposes. Note that the day-to-day variability in the vegetation composition within the footprint is larger at SRER than JER, primarily due to the presence of a large grass area to the north of the EC tower. When the daily flux footprint is focused toward the north (e.g., 18 July), a relatively high grass cover (73.0%) and low velvet mesquite coverage (14.2%) is observed. Contrast this with the typical southerly footprint (e.g., 30 July), which features lower grass (56.6%) and higher velvet mesquite (28.6%) cover. As compared to the surrounding landscape (Table 2), the season-average footprint conditions at SRER have substantially larger fractions of grass cover in the 50% source area, while the JER has a larger proportion of creosote bush and honey mesquite instead of other shrubs. Nevertheless, the day-to-day variability in vegetation composition in the 50% source area (indicated by minimum and maximum values) spans well the conditions found in the seasonally averaged footprints for smaller (30%) and larger (80%) source areas (Table 2).

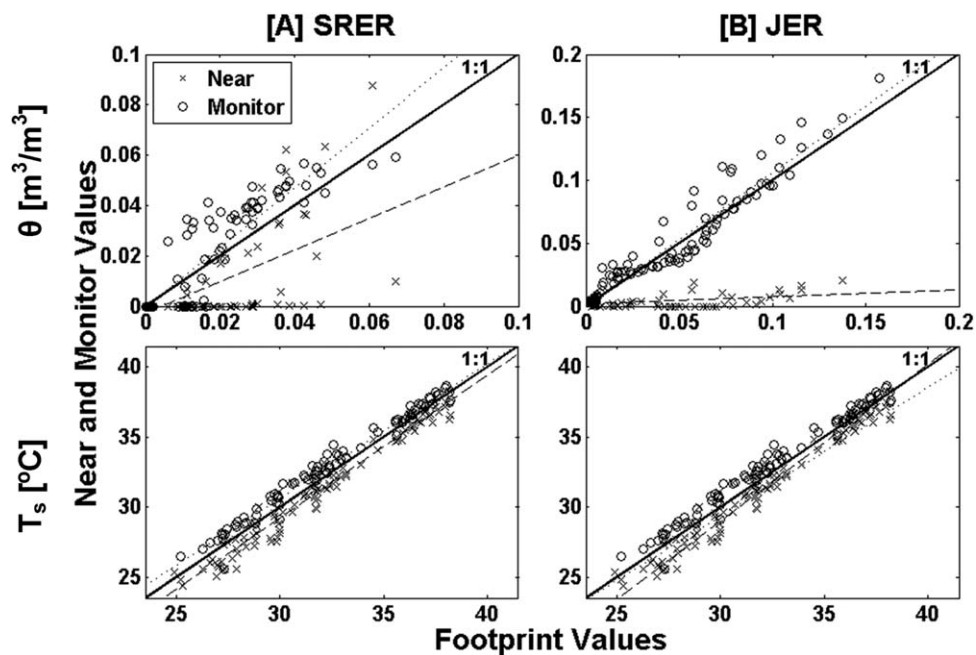


**Figure 6.** Scatterplots of soil moisture ( $\theta$  in  $\text{m}^3/\text{m}^3$ , top) and soil temperature ( $T_s$  in  $^\circ\text{C}$ , bottom) for the 0–10 cm depth average of “Near” and “Monitor” plots as compared to the “Footprint” average at (A) SRER and (B) JER. Solid lines represent the 1:1 line, while dashed lines are linear regressions for the “Near” and “Monitor” plots.

As the daily flux footprint changes with time, contributions from the soil evaporation and plant transpiration are expected to vary. Underlying the ET partitioning method of *Moran et al. [2009]* is the assumption that daily ET is primarily composed of transpiration during periods with large changes in surface temperature and that soil water content increases transpiration. Figure 8 presents the daily ET, T and E for premonsoon (up to 30 June at SRER and 22 July at JER) and monsoon (up to 20 September at SRER and 30 September at JER) periods. The premonsoon period is generally dry, with low ET that is composed primarily of T at SRER, where mesquite trees have fully greened by this time period [*Pierini et al., 2014*], and by E at JER, where the mixed shrubland has species with a phenological cycle tied to the monsoon [*Templeton et al., 2014*]. As a result, T/ET is substantially larger in May and June at SRER than JER (Table 1). During the Monsoon period, both sites exhibit increases in ET (~8 and ~2 mm/d at SRER and JER) with a large transpiration component after significant rainfall events (>20 mm/d) that reach deeper soil layers, whereas small events (<10 mm/d) lead mainly to soil evaporation. Interesting switches occur in the relative magnitudes of T and E depending the sequence of precipitation

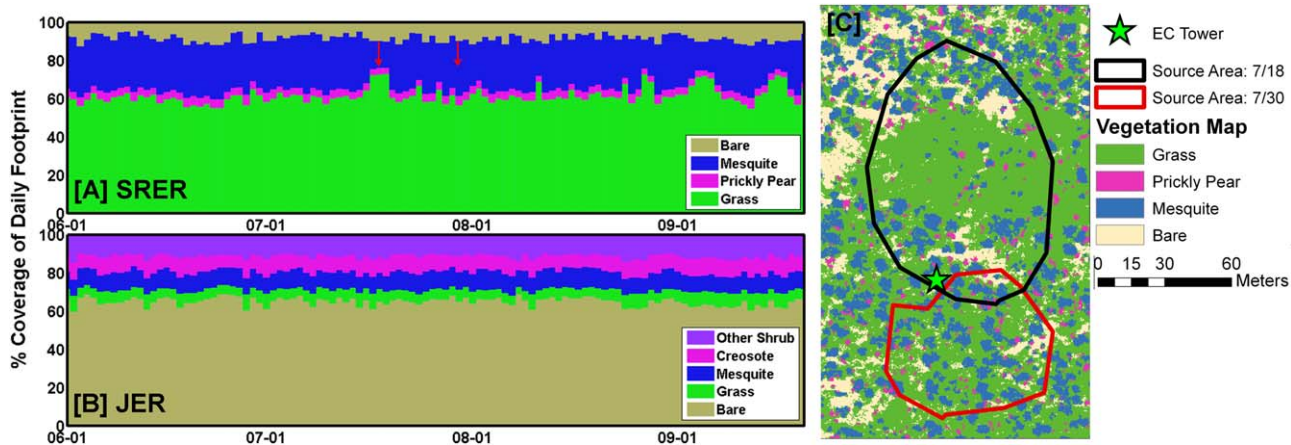


**Figure 7.** Vegetation cover percentage within the daily flux footprint at (A) SRER and (B) JER. Two red arrows in Figure 7A depict days (18 and 30 July) for which the daily flux footprint (50% source area) is shown in Figure 7C for the SRER vegetation distribution. The 50% source area varies from  $14,634 \text{ m}^2$  (18 July) to  $7308 \text{ m}^2$  (30 July), while the maximum fetch distance varies from 120 m (18 July) to 62 m (30 July). Both dates in Figure 7C were selected so that the footprint-average soil moisture was approximately the same at  $\theta = 0.03 \text{ m}^3/\text{m}^3$ .

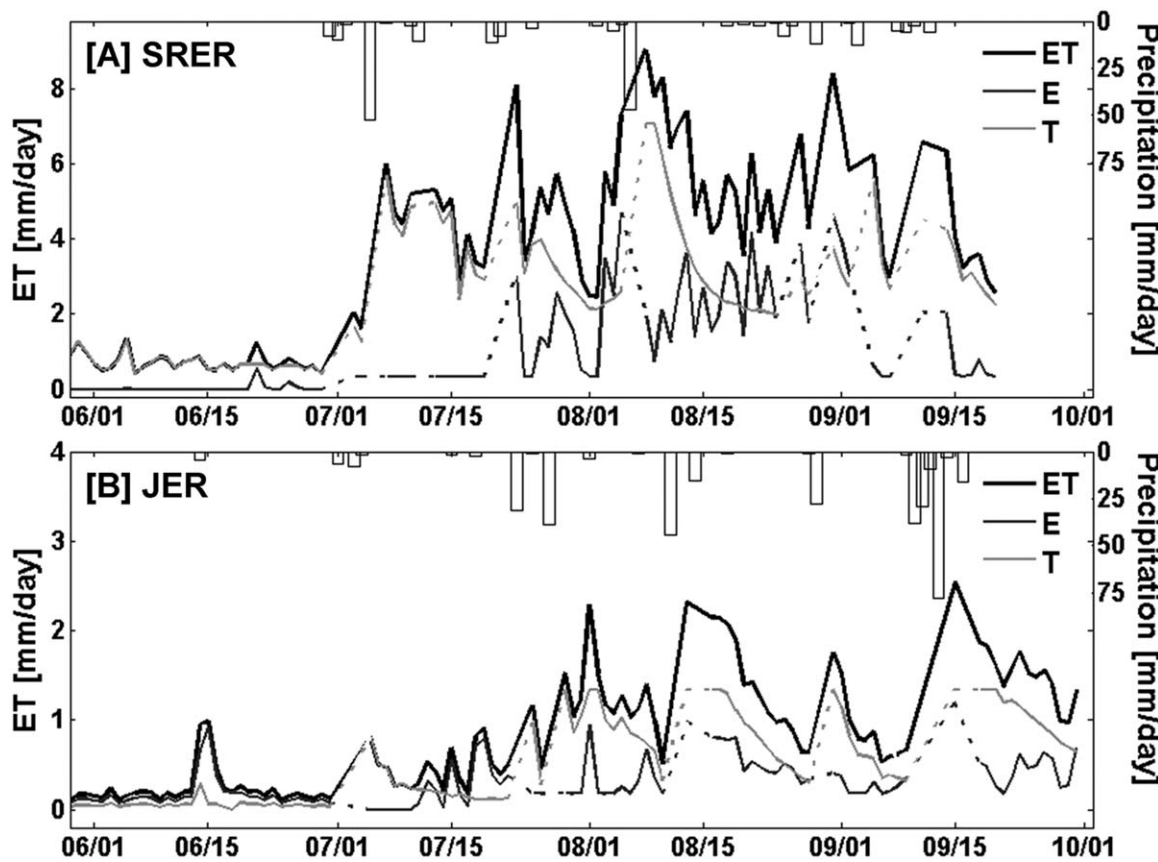


**Figure 8.** Daily evapotranspiration (ET) partitioned into soil evaporation (E) and plant transpiration (T) shown with daily precipitation at (A) SRER and (B) JER. Dashed lines connect valid days for application of the method (i.e., 0–1 day after a  $>5$  mm rainfall were excluded).

events and their characteristics. Overall, SRER had a larger evapotranspiration amount ( $ET/P = 55.0\%$ ) as compared to JER ( $ET/P = 21.7\%$ ), but a smaller  $T/ET$  ratio (59.3 and 68.1% at SRER and JER) during the monsoon period. Thus, while SRER uses available soil water more efficiently (higher  $ET/P$ ) during the summer season than JER, a smaller proportion goes into transpiration, likely due to a larger number of small ( $<10$  mm/d) rainfall events.

### 3.3. Land-Atmosphere Interactions Within Daily Flux Footprint

Monthly and seasonal values of evapotranspiration and its partitioning depend on the daily flux footprint within which contributions of soil and plant patches vary substantially. For instance, the two days shown in Figure 7 (18 and 30 July at SRER) exhibited varying ET (1.4 and 1.7 mm/d) and  $T/ET$  (75 and 50%), despite similar footprint-averaged soil moisture. Thus, while our  $T/ET$  estimates are consistent with prior studies in the region [e.g., Dugas *et al.*, 1996; Reynolds *et al.*, 2000; Scott *et al.*, 2006; Yépez *et al.*, 2007; Méndez-Barroso *et al.*, 2014], a closer inspection is warranted of the controls exerted by vegetation composition. We assessed if explanatory relations exist for  $T/ET$  and EF by testing the mean differences of two populations of vegetation cover using a Student's *t* test, with  $P < 0.1$  indicating a significant relation. The low and high subsets are selected using a certain percentile (i.e., 20, 25, 33, and 40%) of the minimum and maximum cover values. Table 3 presents the results for the monsoon period and for all vegetation cover types for the 20 and 40% percentiles (see Anderson [2013] for the premonsoon period and other percentiles). In addition, we tested if a linear regression slope to the entire data was different from zero at the 0.05 significance level (bolded in Table 3).

Vegetation composition in the daily flux footprint has an important impact on ET partitioning for a selected number of conditions. At SRER, a higher  $T/ET$  occurs for a higher grass cover ( $P = 0.06$  for the 25% percentile), corresponding to a lower mesquite cover ( $P = 0.007$ ). The effect of mesquite cover is also significant for other percentiles (Table 3), though these effects do not hold over the entire range of values as shown

**Table 3.** Student's *t* Tests (P Values) of the Difference in the Mean Values of T/ET and EF Between Low and High Subsets and Linear Regressions (Slope and R<sup>2</sup>) for the Entire Data Set at SRER and JER During the Monsoon Period<sup>a</sup>

Site	Vegetation Cover	Trend Direction	T/ET				EF				
			Subset of Cover Range		Linear Regression		Trend Direction	Subset of Cover Range		Linear Regression	
			20%	40%	Slope	R <sup>2</sup>		20%	40%	Slope	R <sup>2</sup>
SRER	Bare	+	0.682	0.673	0.006	0.01	±	0.608	0.542	-0.51	0.01
	Grass	+	0.242	0.122	0.006	0.03	-	0.112	0.302	-0.57	0.04
	Mesquite	-	<b>0.067</b>	0.407	-0.005	0.03	+	<b>0.072</b>	0.558	0.53	0.04
	Prickly Pear	-	0.346	0.551	-0.052	0.03	+	0.544	0.209	3.56	0.02
	JER	+	0.775	0.507	0.006	0.01	+	<b>0.007</b>	<b>0.001</b>	<b>2.82</b>	0.31
JER	Grass	±	<b>0.076</b>	0.164	-0.014	0.02	-	<b>0.043</b>	<0.001	-4.65	0.23
	Mesquite	+	<b>0.073</b>	0.359	<b>0.031</b>	0.07	+	<b>0.027</b>	<b>0.084</b>	<b>4.61</b>	0.15
	Creosote	+	0.214	0.756	0.005	0.00	-	<b>0.096</b>	0.103	-2.59	0.09
	Other Shrubs	-	<b>0.022</b>	<b>0.017</b>	<b>-0.031</b>	0.10	-	<b>0.029</b>	<b>0.002</b>	-4.95	0.29

<sup>a</sup>Subset cover ranges indicate the percentiles used to determine low and high subsets, while the trend direction indicates if the mean values increase (+), decrease (-) or have no change (±) in direction, with the vegetation cover percentage. Significant Student's *t* test values (*P* < 0.1) and linear regression slopes (0.05 level) are bolded.

through the linear regression test. As a result, when the daily flux footprint is oriented toward the north where a large grass patch is present, a higher T/ET occurs. Nevertheless, EF decreases with grass cover (*P* = 0.093, Table 3). This indicates that large patches of grass and mesquite have measurable impacts on the measured ET and its partitioning at the SRER. At JER, the random distribution of small plants and the higher bare soil fraction lead to different outcomes. T/ET increases with mesquite (*P* = 0.095) cover and decreases with cover of other shrubs (*P* = 0.001) for a number of percentiles (Table 3). Thus, a trade-off occurs as the footprint changes in composition with mesquite leading to higher T/ET, and other shrubs and creosote lowering T/ET. Table 3 also indicate significant increases in EF as bare soil (*P* = 0.003) and mesquite (*P* = 0.017) occupy larger fractions, as substantiated by regression slopes significantly different from zero at the 0.05 level. In contrast, higher grass, creosote, and other shrubs cover decrease EF significantly. As a result, a higher presence of mesquite shrubs increases total ET and T/ET, while other vegetation decreases ET.

We now turn attention to the linkages between land surface states ( $\theta$  and  $T_s$ ) and turbulent fluxes (ET and H). Figures 9 and 10 present daytime relations of  $ET = f(\theta)$  and  $H = f(T_s)$  obtained for the entire study period,

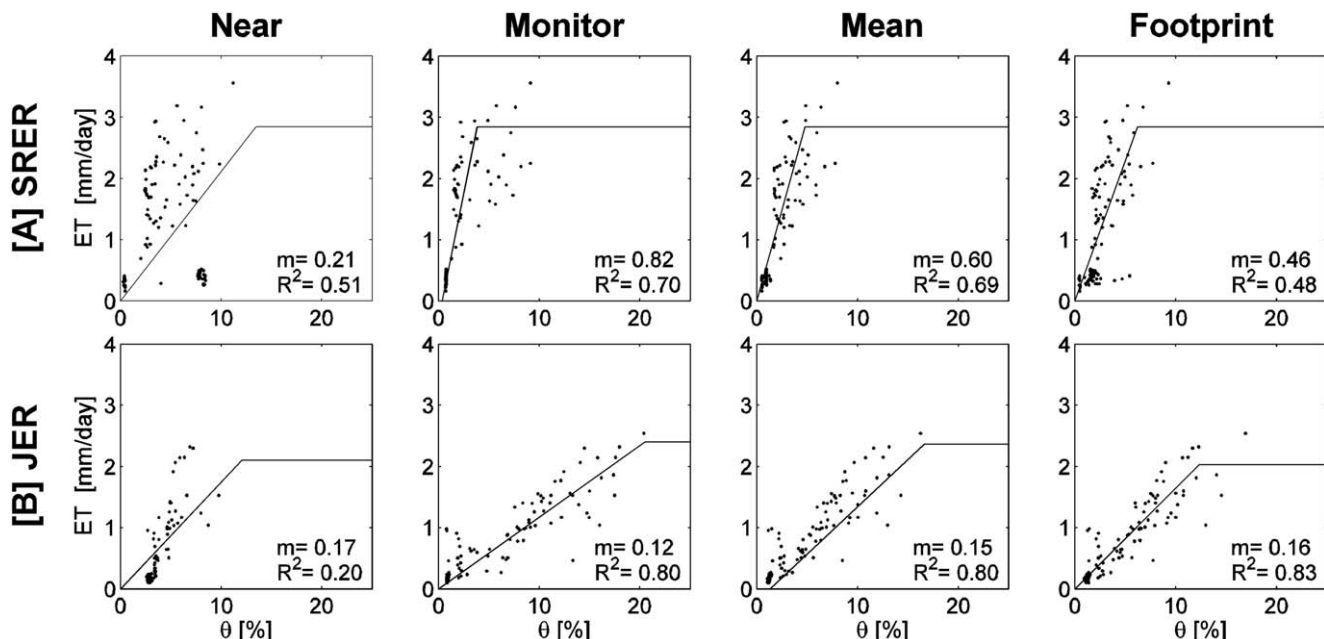


**Figure 9.** Daily evapotranspiration (ET) as a function of soil moisture ( $\theta$  in %, 0–20 cm depth average) based on four methods at (A) SRER and (B) JER. A piecewise linear regression is performed for each case, with resulting ramp slope ( $m$ ) and  $R^2$  values shown.

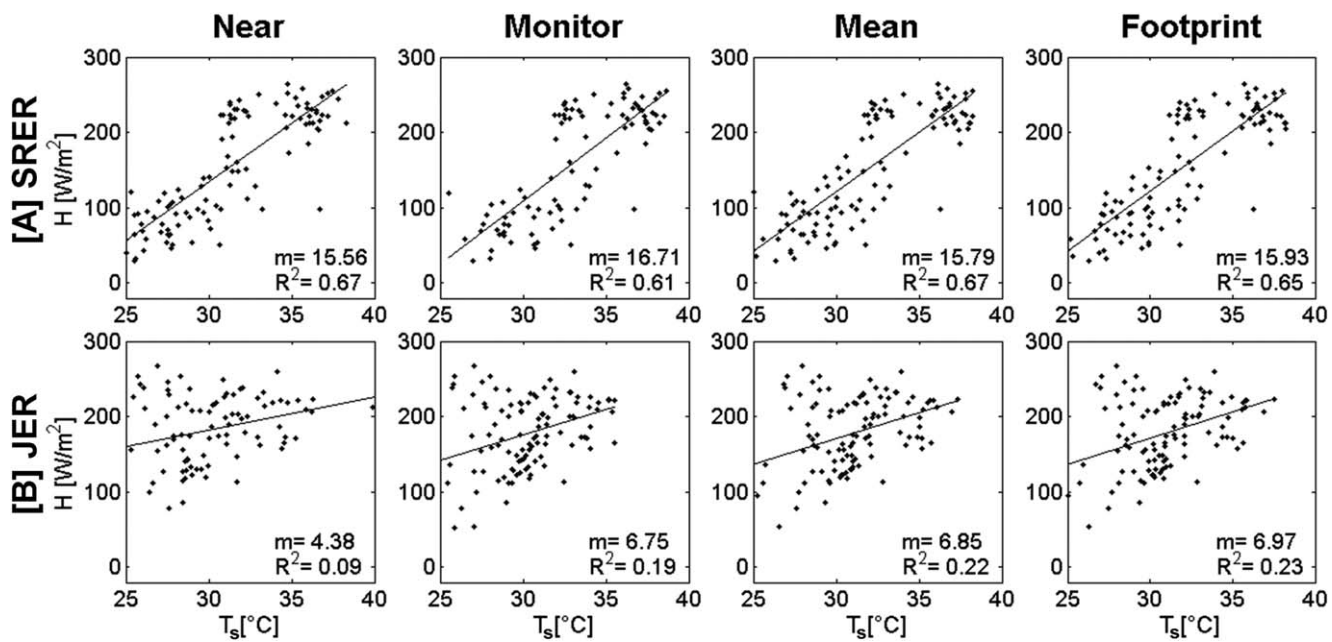


**Figure 10.** Daytime sensible heat flux (H) as a function of soil temperature (T<sub>s</sub> in °C, 0–10 cm depth average) based on four methods at (A) SRER and (B) JER. A linear regression is performed for each case, with resulting ramp slope (m) and R<sup>2</sup> values shown.

excluding 0–1 days after a significant rainfall event (>5 mm). Comparison of the four approaches (“Near,” “Monitor,” “Mean,” “Footprint”) to estimate θ and T<sub>s</sub> is used to identify the effect of the scale of the land surface states. Table 4 presents regression parameters over all depth averages, while Figures 9 and 10 depict selected values (0–20 cm θ and 0–10 cm T<sub>s</sub>). Typically, the coefficient of determination (R<sup>2</sup>) improves for ET = f(θ) for larger depth averages (i.e., deeper soil moisture has a stronger control on ET), whereas R<sup>2</sup> decreases for H = f(T<sub>s</sub>) for larger soil depth averages (i.e., H is more closely linked to surface T<sub>s</sub>). Furthermore, a marked improvement is observed between the cases that capture the variability in the daily flux footprint (“Monitor,” “Mean,” “Footprint”) as compared to the use of a single plot (“Near”). This indicates that capturing the spatial variability of θ and T<sub>s</sub> is critical for relating land surface conditions to turbulent fluxes. In addition, the improvement in R<sup>2</sup> achieved when capturing conditions around the EC tower is larger for θ than T<sub>s</sub>, consistent with the time-stability analysis. While differences in “Monitor,” “Mean,” and “Footprint” are small, the “Footprint” approach has better ET = f(θ) and H = f(T<sub>s</sub>) relations at JER since the spatial variability in θ and T<sub>s</sub> is higher than at SRER (i.e., improvement in R<sup>2</sup> using “Footprint” as compared to “Near” is larger at JER).

**Table 4.** Statistical Parameters (Ramp Slope, m, and Coefficient of Determination, R<sup>2</sup>) for Relations Between Daily Turbulent Fluxes (ET and H) and Land Surface States (θ and T<sub>s</sub>) Estimated Through Four Methods (“Near,” “Monitor,” “Mean,” and “Footprint”) for Three Depth Averaging Intervals

Relation	Site	Depth (cm)	Near		Monitor		Mean		Footprint	
			m	R <sup>2</sup>	m	R <sup>2</sup>	m	R <sup>2</sup>	m	R <sup>2</sup>
ET and θ	SRER	0–10	0.89	0.20	0.51	0.19	0.90	0.60	1.01	0.28
		0–20	0.21	0.51	0.82	0.70	0.60	0.69	0.46	0.48
		0–40	0.21	0.50	0.53	0.62	0.48	0.64	0.40	0.62
	JER	0–10	0.91	0.64	0.17	0.67	0.18	0.76	0.18	0.79
		0–20	0.17	0.20	0.12	0.80	0.15	0.80	0.16	0.83
		0–40	0.14	0.06	0.17	0.77	0.16	0.78	0.16	0.79
H and T <sub>s</sub>	SRER	0–10	15.56	0.67	16.71	0.61	15.79	0.67	15.93	0.65
		0–20	16.82	0.63	17.68	0.59	16.82	0.61	16.81	0.60
		0–40	18.74	0.56	19.27	0.49	18.45	0.52	18.63	0.51
	JER	0–10	4.38	0.09	6.75	0.19	6.85	0.22	6.97	0.23
		0–20	3.13	0.03	6.30	0.16	6.56	0.17	6.83	0.18
		0–40	-1.62	0.01	5.16	0.09	5.27	0.08	5.49	0.09

A comparison of the relations of turbulent fluxes and land surface states in the semiarid ecosystems is also instructive. Overall, turbulent fluxes in the SRER savanna are more sensitive to changes in the land surface states, as indicated by the slope ( $m$ ), with more pronounced increases in ET (0 to  $\sim 3.5$  mm/d) at smaller values of  $\theta$  (0 to  $\sim 10\%$ , Figure 9) and a larger range of  $H$  ( $\sim 30$ – $250$  W/m $^2$ ) within the variations of  $T_s$  (25–38°C, Figure 10), as compared to JER. This is linked to the two main differences between the study sites, namely that: (1) SRER had summer conditions similar to the long-term average and (2) its vegetation consisted of large, homogeneous patches. First, the near-average precipitation at SRER led to a drier and hotter land surface state relative to JER. As a result, storm events significantly moistened and cooled the surface, leading to a stronger connection with the turbulent fluxes (i.e., a larger sensitivity of ET and  $H$  to  $\theta$  and  $T_s$ ). The mixed shrubland at JER, on the other hand, had above-average rainfall, such that the land surface was wetter and cooler than average. This led to a looser coupling of turbulent fluxes with land surface states (i.e., less sensitivity of ET to  $\theta$  as other factors played a role). Second, the larger, homogeneous plant patches at SRER implied that variations in the size and location of the daily flux footprint mattered more substantially than at JER. This occurs despite that SRER had smaller spatial variations in land surface conditions since the vegetation classes (i.e., grass versus mesquite) have substantially different behaviors. In contrast, the higher spatial variability at JER under the above-average precipitation occurs in a more random pattern around the EC tower with no preferential directions due to the smaller plant and bare soil patches, leading to a lower sensitivity of turbulent fluxes to the land surface patterns.

#### 4. Summary and Conclusions

Modern techniques for assessing relations between turbulent fluxes and land surface states rely on measurements obtained at disparate spatial scales. While this may be a reasonable assumption in some settings, water-limited ecosystems exhibit heterogeneities in vegetation and soil cover that preclude this simple treatment. In this study, we used data sets from two semiarid ecosystems to quantify the spatial variability in soil moisture and temperature in the daily flux footprint derived from an analytical model. The cross-site comparison was used to determine how land-atmospheric coupling varied with the differences in the land surface state conditions and vegetation composition at each site. To our knowledge, this is the first systematic attempt to quantify how the spatiotemporal variability of land surface states impact turbulent fluxes in the eddy covariance source area. The conclusions of the study can be summarized as:

1. The spatiotemporal variability of  $\theta$  and  $T_s$  in the daily flux footprint was substantial in both ecosystems. However, the random distribution of smaller soil and shrub patches at JER led to more varied conditions as compared to SRER, in particular for  $\theta$  (e.g., standard deviation of 7.66 and 3.60% at JER and SRER). Wetter surface soils were present at JER as compared to SRER, in response to the above-average precipitation, though average soil temperatures were similar. A higher spatial variability in  $\theta$  as compared to  $T_s$  resulted in a poorer performance for single plots in representing the flux footprint conditions for soil moisture in these ecosystems.
2. Overall, SRER had a larger evapotranspiration amount (ET = 116.2 mm) as compared to JER (ET = 77.1 mm), but a smaller T/ET ratio (59.3 and 68.1% at SRER and JER) after the onset of the monsoon. Thus, while the savanna at SRER used soil water more efficiently than the mixed shrubland at JER (i.e., ET/P = 55.0 and 21.7% at SRER and JER), a smaller proportion occurred as T, likely due to small rainfall events promoting E.
3. Daily variations in vegetation within the flux footprint were higher at SRER than at JER, due to the presence of a large grass area at SRER and a more random pattern of shrub and bare soil cover at JER. The vegetation composition in the daily flux footprint was found to have an important impact on ET and its partitioning in both ecosystems. For instance, a higher ET and E/ET was found for low mesquite cover in the footprint at SRER, while a higher ET and T/ET occurred for a higher mesquite coverage at JER. As a result, quantifiable linkages exist between the flux footprint vegetation composition and the measured ET and its estimated components.
4. A marked improvement in land-atmosphere relations was found for those methods capturing the spatial variability in the daily flux footprint as compared to the use of a single plot. Improvements were more significant for  $\theta$  as this varied more prominently than  $T_s$ , and at JER, where the spatial variability in  $\theta$  and  $T_s$  was larger than at SRER. Overall, turbulent fluxes at SRER were more sensitive to changes in land surface states as compared to JER due to its overall drier conditions and the larger changes in vegetation composition with distinct behaviors.

Characterized by the process of woody plant encroachment, the studied ecosystems represent large expanses of land in the Sonoran and Chihuahuan Deserts used as rangelands. As a result, the study findings are relevant for a

broad range of applications aimed at determining the contribution of rangelands to regional climate [e.g., Beltran-Przekurat *et al.*, 2008], water supply [e.g., Wainwright *et al.*, 2000], and other ecosystem services [e.g., Yahdjian *et al.*, 2015]. Under current rangeland practices, semiarid ecosystems in the southwestern U.S. will continue to change in spatial patterns and composition [e.g., Archer *et al.*, 1995; Browning *et al.*, 2008]. As a result, it is imperative to account for the spatial and temporal variations in the vegetation and bare soil patches that characterize these ecosystems and their associated land surface states, as these can have measurable impacts on land-atmosphere interactions.

### Acknowledgments

We thank two anonymous reviewers whose insightful comments helped to improve the manuscript. Funding for this effort was provided by the U.S. Army Research Office (grant 56059-EV-PCS) and the Jornada Long Term Ecological Research (National Science Foundation grant DEB-1235828). We thank Nicole A. Pierini and Adam Schreiner-McGraw for help during field activities and Giuseppe Mascaro for advice on statistical analyses. Data sets are available through the Jornada Data Catalog at <http://jornada.nmsu.edu/data-catalogs/jornada>.

### References

- Alfieri, J. G., and P. D. Blanken (2012), How representative is a point? The spatial variability of surface energy fluxes across short distances in a sand-sagebrush ecosystem, *J. Arid Environ.*, 87, 42–49.
- Alfieri, J. G., P. D. Blanken, D. N. Yates, and K. Steffen (2007), Variability in the environmental factors driving evapotranspiration from a grazed rangeland during severe drought conditions, *J. Hydrometeorol.*, 2, 207–220.
- Anderson, C. A. (2013), Assessing land-atmosphere interactions through distributed footprint sampling at two eddy covariance towers in semiarid ecosystems of the Southwestern U.S., MS thesis, 243 pp., Dept. of Civ., Environ. and Sustainable Eng., Ariz. State Univ., Tempe. [Available at <http://repository.asu.edu/items/21017>.]
- Archer, S., D. S. Schimel, and E. A. Holland (1995), Mechanisms of shrubland expansion: Land use, climate or CO<sub>2</sub>, *Clim. Change*, 29, 91–99.
- Archer, S., T. W. Boutton, and K. A. Hibbard (2001), Trees in grasslands: Biogeochemical consequences of woody plant expansion, in *Global Biogeochemical Cycles in the Climate System*, edited by E.-D. Schulze *et al.*, pp. 115–138, Academic, San Diego, Calif.
- Baldocchi, D. (2008), Breathing of the terrestrial biosphere: Lessons learned from a global network of carbon dioxide flux measurement systems, *Aust. J. Bot.*, 56, 1–26.
- Baldocchi, D., B. B. Hicks, and T. P. Meyers (1988), Measuring biosphere-atmosphere exchanges of biologically related gases with micrometeorological method, *Ecology*, 69, 1331–1340.
- Beltran-Przekurat, A., R. A. Pielke, D. P. C. Peters, K. A. Snyder, and A. Rango (2008), Modeling the effects of historical vegetation change on near-surface atmosphere in the northern Chihuahuan Desert, *J. Arid Environ.*, 72(10), 1897–1910.
- Blanken, P. D., T. A. Black, H. H. Neumann, G. den Hartog, P. C. Yang, Z. Nesic, and X. Lee (2001), The seasonal water and energy exchange above and within a boreal aspen forest, *J. Hydrol.*, 245, 118–136.
- Browning, D. M., S. R. Archer, G. P. Asner, M. P. McClaran, and C. A. Wessman (2008), Woody plants in grasslands: Post-encroachment stand dynamics, *Ecol. Appl.*, 18(4), 928–944.
- Burrows, W. H., J. O. Carter, J. C. Scanlan, and E. R. Anderson (1990), Management of savannas for livestock production in north-east Australia: Contrasts across the tree grass continuum, *J. Biogeogr.*, 17(4/5), 503–512.
- Campbell, J. E. (1990), Dielectric properties and influence of conductivity in soils at one to fifty Megahertz, *Soil Sci. Soc. Am. J.*, 54, 332–341.
- Chesson, P., R. L. E. Gebauer, S. Schwinnning, N. Huntly, K. Wiegand, M. S. K. Ernest, A. Sher, A. Novoplansky, and J. E. Weltzin (2004), Resource pulses, species interactions, and diversity maintenance in arid and semi-arid environments, *Oecologia*, 141, 236–253.
- Clement, R. (1999), *EdiRe Data Software* (Version 1.5.0.32), Sch. of Geosci., Univ. of Edinburgh, Edinburgh, U.K. [Available at <http://www.geos.ed.ac.uk/abs/research/micromet/EdiRe>.]
- Delhomme, J. P. (1978), Kriging in the hydrosciences, *Adv. Water Resour.*, 1, 251–266.
- Detto, M., N. Montaldo, J. D. Albertson, M. Mancini, and G. Katul (2006), Soil moisture and vegetation controls on evapotranspiration in a heterogeneous Mediterranean ecosystem on Sardinia, Italy, *Water Resour. Res.*, 42, W08419, doi:10.1029/2005WR004693.
- D'Odorico, P., G. S. Okin, and B. T. Bestelmeyer (2012), A synthetic review of feedbacks and drivers of shrub encroachment in arid grasslands, *Ecohydrology*, 5, 520–530.
- Douglas, M. W., R. A. Maddox, K. Howard, and S. Reyes (1993), The Mexican monsoon, *J. Clim.*, 6(8), 1665–1677.
- Dugas, W. A., R. A. Hicks, and R. P. Gibbens (1996), Structure and function of C3 and C4 Chihuahuan Desert plant communities: Energy balance components, *J. Arid Environ.*, 34, 63–79.
- Evett, S. R., W. P. Kustas, P. H. Gowda, M. C. Anderson, J. H. Prueger, and T. A. Howell (2012), Overview of the Bushland Evapotranspiration and Agricultural Remote sensing Experiment 2008 (BEAREX08): A field experiment evaluating methods of quantifying ET at multiple scales, *Adv. Water Resour.*, 50, 4–19.
- Gelybo, G., Z. Barcza, A. Kern, and N. Kijun (2013), Effect of spatial heterogeneity on the validation of remote sensing based GPP estimations, *Agric. For. Meteorol.*, 174–175, 43–53.
- Gockede, M., C. Rebmann, and T. Foken (2004), A combination of quality assessment tools for eddy covariance measurements with footprint modelling for the characterisation of complex sites, *Agric. For. Meteorol.*, 127, 175–188.
- Grayson, R. B., and A. W. Western (1998), Towards areal estimation of soil water content from point measurements: Time and space stability of mean response, *J. Hydrol.*, 207, 68–82.
- Hsieh, C.-I., G. Katul, and T. Chi (2000), An approximate analytical model for footprint estimation of scalar fluxes in thermally stratified atmospheric flows, *Adv. Water Resour.*, 23, 765–772.
- Huenneke, L. F., J. P. Anderson, M. Remmenga, and W. H. Schlesinger (2002), Desertification alters patterns of aboveground net primary production in Chihuahuan ecosystems, *Global Change Biol.*, 8(3), 247–264.
- Huxman, T. E., B. P. Wilcox, D. D. Breshears, R. L. Scott, K. A. Snyder, E. E. Small, K. Hultine, W. T. Pockman, and R. B. Jackson, (2005), Ecohydrological implications of woody plant encroachment, *Ecology*, 86(2), 308–319.
- Ivanov, V. Y., E. R. Vivoni, R. L. Bras, and D. Entekhabi (2004), Catchment hydrologic response with a fully-distributed triangulated irregular network model, *Water Resour. Res.*, 40, W11102, doi:10.1029/2004WR003218.
- Kormann, R., and F. X. Meixner (2001), An analytical footprint model for non-neutral stratification, *Boundary Layer Meteorol.*, 99, 207–224.
- Kurc S. A., and E. E. Small (2007), Soil moisture variations and ecosystem-scale fluxes of water and carbon in semiarid grassland and shrubland, *Water Resour. Res.*, 43, W06416, doi:10.1029/2006WR005011.
- Laio, F., A. Porporato, L. Ridolfi, and I. Rodriguez-Iturbe (2001), Plants in water-controlled ecosystems: Active role in hydrologic processes and response to water stress II. Probabilistic soil moisture dynamics, *Adv. Water Resour.*, 24, 707–723.
- Li, F., W. P. Kustas, M. C. Anderson, J. H. Prueger, and R. L. Scott (2008), Effect of remote sensing spatial resolution on interpreting tower-based flux observations, *Remote Sens. Environ.*, 112, 337–349.

- Lloyd, C. R., P. Bessemoulin, F. D. Cropley, A. D. Culf, A. J. Dolman, J. Elbers, B. Heusinkveld, J. B. Moncrieff, B. Monteny, and A. Verhoef (1997), A comparison of surface fluxes at the HAPEX-Sahel fallow bush sites, *J. Hydrol.*, 188–189, 400–425.
- Loescher, H., E. Ayres, P. Duffy, H. Luo, and M. Brunke (2014), Spatial variation in soil properties among North American ecosystems and guidelines for sampling designs, *PLoS One*, 9(1), e83216.
- Marcolla, B., and A. Cescatti (2005), Experimental analysis of flux footprint for varying stability conditions in an alpine meadow, *Agric. For. Meteorol.*, 135, 291–301.
- Massman, W. J. (2001), Reply to comment by Rannik on: "A simple method for estimating frequency response corrections for eddy covariance systems," *Agric. For. Meteorol.*, 107, 247–251.
- Méndez-Barroso, L. A., E. R. Vivoni, A. Robles-Morua, E. A. Yépez, J. C. Rodríguez, C. J. Watts, J. Garatuza-Payán, and J. A. Saiz-Hernandez (2014), A modeling approach reveals differences in evapotranspiration and its partitioning in two semiarid ecosystems in northwest Mexico, *Water Resour. Res.*, 50, 3229–3252.
- Montgomery, D. C., G. C. Runger, and N. F. Hubele (2006), *Engineering Statistics*, 4th ed., 512 pp., John Wiley, Hoboken, N. J.
- Moran, M. S., R. L. Scott, T. O. Keefer, W. E. Emmerich, M. Hernandez, G. S. Nearing, G. B. Paige, M. H. Cosh, and P. E. O'Neill (2009), Partitioning evapotranspiration in semiarid grassland and shrubland ecosystems using time series of soil surface temperature, *Agric. For. Meteorol.*, 149, 59–72.
- Ogle, K., and J. F. Reynolds (2004), Plant responses to precipitation in desert ecosystems: Integrating functional types, pulses, thresholds and delays, *Oecologia*, 141, 282–294.
- Pierini, N. A., E. R. Vivoni, A. Robles-Morua, R. L. Scott, and M. A. Nearing (2014), Using observations and a distributed hydrologic model to explore runoff thresholds linked with mesquite encroachment in the Sonoran Desert, *Water Resour. Res.*, 50, 8191–8215, doi:10.1002/2014WR015781.
- Reynolds, J. F., R. A. Virginia, P. R. Kemp, A. G. de Soya, and D. C. Tremmel (1999), Impact of drought on desert shrubs: Effects of seasonality and degree of resource island development, *Ecol. Monogr.*, 69, 69–106.
- Reynolds, J. F., P. R. Kemp, and J. D. Tenhunen (2000), Effects of long-term rainfall variability on evapotranspiration and soil water distribution in the Chihuahuan Desert: A modeling analysis, *Plant Ecol.*, 150, 145–159.
- Running, S. W., D. D. Baldocchi, D. P. Turner, S. T. Gower, P. S. Bakwin, and K. A. Hibbard (1999), A global terrestrial monitoring network integrating tower fluxes, flask sampling, ecosystem modeling and EOS satellite data, *Remote Sens. Environ.*, 70, 108–127.
- Schmid, H. P. (2002), Footprint modeling for vegetation atmosphere exchange studies: A review and perspective, *Agric. For. Meteorol.*, 113, 159–183.
- Scholes, R. J., and S. R. Archer (1997), Tree-grass interactions in savannas, *Annu. Rev. Ecol. Syst.*, 28(1), 517–544.
- Scott, R. L., E. A. Edwards, W. J. Shuttleworth, T. E. Huxman, C. J. Watts, and D. C. Goodrich (2004), Interannual and seasonal variations in fluxes of water and carbon dioxide from a riparian woodland ecosystem, *Agric. For. Meteorol.*, 122, 64–84.
- Scott, R. L., T. E. Huxman, W. L. Cable, and W. E. Emmerich (2006), Partitioning of evapotranspiration and its relation to carbon dioxide exchange in a Chihuahuan desert shrubland, *Hydro. Processes*, 20(15), 3227–3243.
- Seyfried, M. S., L. E. Grant, E. Du, and K. Humes (2005), Dielectric loss and calibration of the Hydra probe soil water sensor, *Vadose Z. J.*, 4, 1070–1079.
- Silva, J. F., A. Zambrano, and M. Farinas (2001), Increase in the woody component of seasonal savannas under different fire regimes in Calabozo, Venezuela, *J. Biogeogr.*, 28(8), 977–983.
- Templeton, R. C., E. R. Vivoni, L. A. Méndez-Barroso, N. A. Pierini, C. A. Anderson, A. Rango, A. S. Laliberte, and R. L. Scott (2014), High-resolution characterization of a semiarid watershed: Implications on evapotranspiration estimates, *J. Hydrol.*, 509, 306–319.
- Twine, T. E., W. P. Kustas, D. R. Cook, P. R. Houser, T. P. Meyers, J. H. Prueger, P. J. Starks, and M. L. Wesely (2000), Correcting eddy-covariance flux underestimates over a grassland, *Agric. For. Meteorol.*, 103, 279–300.
- Van Auken, O. W. (2000), Shrub invasions of North American semiarid grasslands, *Annu. Rev. Ecol. Syst.*, 31(1), 197–215.
- Vivoni, E. R. (2012), Diagnosing seasonal vegetation impacts on evapotranspiration and its partitioning at the catchment scale during SMEX04, *J. Hydrometeorol.*, 13, 1631–1638.
- Vivoni, E. R., H. A. Moreno, G. Mascaro, J. C. Rodríguez, C. J. Watts, J. Garatuza-Payán, and R. L. Scott (2008a), Observed relation between evapotranspiration and soil moisture in the North American monsoon region, *Geophys. Res. Lett.*, 35, L22403, doi:10.1029/2008GL036001.
- Vivoni, E. R., M. Gebremichael, C. J. Watts, R. Bindlish, and T. J. Jackson (2008b), Comparison of ground-based and remotely-sensed surface soil moisture estimates over complex terrain during SMEX04, *Remote Sens. Environ.*, 112(2), 314–325.
- Vivoni, E. R., C. J. Watts, J. C. Rodríguez, J. Garatuza-Payán, L. A. Méndez-Barroso, and J. A. Saiz-Hernandez (2010), Improved land-atmosphere relations through distributed footprint sampling in a subtropical scrubland during the North American monsoon, *J. Arid Environ.*, 74, 579–584.
- Wainwright, J., A. J. Parsons, and A. D. Abrahams (2000), Plot-scale studies of vegetation, overland flow and erosion interactions: Case studies from Arizona and New Mexico, *Hydro. Processes*, 14(16–17), 2921–2943.
- Webb, E. K., G. I. Pearman, and R. Leuning (1980), Correction of flux measurements for density effects due to heat and water vapour transfer, *Q. J. R. Meteorol. Soc.*, 106, 85–100.
- Wilczak, J. M., S. P. Oncley, and S. A. Stage (2001), Sonic anemometer tilt correction algorithms, *Boundary Layer Meteorol.*, 99, 127–150.
- Williams, C. A., and J. D. Albertson (2004), Soil moisture controls on canopy-scale water and carbon fluxes in an African savanna, *Water Resour. Res.*, 40, W09302, doi:10.1029/2004WR003208.
- Williams, D. G., et al. (2004), Evapotranspiration components determined by stable isotope, sap flow and eddy covariance techniques, *Agric. For. Meteorol.*, 125, 241–258.
- Yahdjian, L., O. E. Sala, and K. M. Havstad (2015), Rangeland ecosystem services: Shifting focus from supply to reconciling supply and demand, *Front. Ecol. Environ.*, 13(1), 44–51.
- Yépez, E., R. L. Scott, W. Cable, and D. Williams (2007), Intraseasonal variation in water and carbon dioxide flux components in a semiarid riparian woodland, *Ecosystems*, 10, 1100–1115.